

Test of Fermi gas model and plane-wave impulse approximation against electron-nucleus scattering data

A.V. Butkevich and S.P. Mikheyev[†]

Institute for Nuclear Research, Russian Academy of Science,
60th October Anniversary p.7A, Moscow 117312, Russia
(Dated: April 16, 2024)

A widely used relativistic Fermi gas model and plane-wave impulse approximation approach are tested against electron-nucleus scattering data. Inclusive quasi-elastic cross section are calculated and compared with high-precision data for ^{12}C , ^{16}O , and ^{40}Ca . A dependence of agreement between calculated cross section and data on a momentum transfer is shown. Results for the $^{12}\text{C}(\text{e}, \text{e}')(\text{p})$ reaction are presented and compared with experimental data of the LSND collaboration.

PACS numbers: 25.30.Bf, 25.30.Pt, 13.15.+g, 24.10.Jv

I. INTRODUCTION

A precise description of neutrino-nucleus (A) interactions in intermediate energy region is important for the interpretation of measurements by many neutrino experiments. The understanding of their sensitivity to neutrino properties, evaluation of the neutrino fluxes and spectra depend on the accuracy to which the A cross sections are known. This is in particular crucial in analysis of the long-baseline neutrino oscillation experiments in which the parameter of neutrino oscillation θ_{12}^2 is determined using the total number of detected events and the distortions in the energy distribution of the detected muons caused by neutrino oscillation. On the other hand the neutrino-nucleus cross sections contain contributions from both axial-vector and vector currents and thus provide complementary information to that provided by electron-nucleus scattering, which is sensitive only to the nuclear vector current.

In many experiments the neutrino fluxes in sub-GeV and GeV energy region are used. At such energies the charged-current quasi-elastic (QE) neutrino-nucleus interactions give the main contribution to the detected events. Sizable nuclear effects have been observed in lepton scattering off nucleus at energies less than a few GeV. They indicate that the nuclear environment plays an important role even at energies and momenta larger than those involved in typical nuclear ground state processes. The understanding of nuclear effects is relevant for the long-baseline neutrino experiments in order to control the corresponding systematic uncertainties.

Many Monte-Carlo (MC) [1] codes developed for simulation of the neutrino detectors response are based on a simple picture of a nucleus as a system of quasi-free nucleons, i.e. a relativistic Fermi gas model (RFGM) [2]. It takes into account Fermi motion of nucleons inside the nucleus and Pauli blocking effect. Unfortunately

the uncertainties of a few A scattering data at low and intermediate energies don't allow us to estimate the accuracy of this model. On the other hand, as follows from vast high-precision electron scattering data the RFGM neglects some important nuclear effects. So, the model which is used for calculation of neutrino scattering off nucleus should first be tested against electron scattering data.

In the present work we intent to evaluate the accuracy of the Fermi gas model and plane-wave impulse approximation (PWIA) [3,4,5]. The electron QE cross sections are calculated in the framework of these models and compared with high-precision data for different nuclei. This comparison shows that the agreement between predictions of these models and data depends significantly on the momentum transfer to the target. We applied the RFGM and plane-wave impulse approximation to $^{12}\text{C}(\text{e}, \text{e}')(\text{p})$ reaction also.

The formalism of an inclusive charged current lepton-nucleus QE scattering is given in Sec.2. Results are presented and discussed in Sec.3 and some conclusions are drawn in Sec.4.

II. FORMALISM OF THE INCLUSIVE QUASI-ELASTIC SCATTERING

In electromagnetic and weak charge current process electrons (neutrinos) interact with nuclei via the exchange of photons or W -boson and charged leptons are produced in the final state. In an inclusive reaction, in which incident electron (e^{el}) or neutrino (e^{cc}) with four-momentum $k_i = (E_i; \mathbf{k}_i)$ is absorbed by nucleus with mass m_A and only the out-going lepton with four-momentum $k_f = (E_f; \mathbf{k}_f)$ and mass m_l is detected, the cross section is given by contracting the lepton tensor and the nuclear tensor

$$d\sigma^{\text{el}} = \frac{1}{Q^4} \frac{1}{j_f j_i} L^{(\text{el})} W^{(\text{el})} d^3k_f; \quad (1)$$

[†]Electronic address: butkevich@inr.ru

[†]Electronic address: mikheyev@pcmail0.inr.ru

$$d^{cc} = \frac{G^2 \cos^2 \theta_c}{2} \frac{1}{\mu_f} L^{(cc)} W^{(cc)} \frac{d^3 k_f}{(2\pi)^2}; \quad (2)$$

where $\theta_c = 137^\circ$ is the fine-structure constant, $G_F = 1.16639 \cdot 10^{-11} \text{ MeV}^{-2}$ is the Fermi constant, θ_c is the Cabibbo angle ($\cos \theta_c = 0.9749$), $Q^2 = q^2 = (k_i - k_f)^2$, and $q = (!; q)$ is the four-momentum transfer.

The lepton tensor can be written, by separating the symmetrical l_S and antisymmetrical components l_A as follows

$$L^{(el)} = l_S; \quad L^{(cc)} = l_S + l_A; \quad (3)$$

$$l_S = 2(k_i k_f + k_f k_i - g k_i k_i); \quad (4)$$

$$l_A = 2i \epsilon_{ijk} k_i k_j; \quad (5)$$

where ϵ_{0123} is the antisymmetric tensor with $\epsilon_{0123} = 1$. Assuming the reference frame in which the z-axis is parallel to the momentum transfer $q = k_i - k_f$ and the y-axis is parallel to $k_i - k_f$, the symmetrical components $l_S^{0x}; l_S^{xy}; l_S^{zy}$ and the antisymmetrical ones $l_A^{0x}; l_A^{xz}; l_A^{0z}$, as well as those obtained from them by exchanging their indices, vanish.

The electromagnetic $W^{(el)}$ and weak charged-current $W^{(cc)}$ hadronic tensors are given by bilinear products of the transition matrix elements of the nuclear electromagnetic (weak charged current) operator $J^{(el)(cc)}$ between the initial nucleus state $|i\rangle$ of energy E_0 and final state $|f\rangle$ of energy E_f as

$$W^{(el)(cc)} = \sum_f \langle i | J^{(el)(cc)} | f \rangle \langle f | J^{(el)(cc)} | i \rangle \quad (E_0 + ! - E_f); \quad (6)$$

where the sum is taken over the undetected states.

The transition matrix elements are calculated in the first order perturbation theory and in impulse approximation, i.e. assuming that the incident lepton interacts with the single nucleon while other ones behave as spectators. The nuclear current operator $J^{(el)(cc)}(q)$ is taken as the sum of single-nucleon currents $j^{(el)(cc)}(q)$, i.e.

$$J^{(el)(cc)} = \sum_{i=1}^A j_i^{(el)(cc)};$$

with

$$j^{(el)} = F_V(Q^2) + \frac{i}{2M} F_M(Q^2) \not{q}; \quad (7)$$

$$j^{(cc)} = F_V(Q^2) + \frac{i}{2M} F_M(Q^2) \not{q} + F_A(Q^2) \gamma_5 + F_P(Q^2) \not{q} \gamma_5; \quad (8)$$

where M is the nucleon mass and $\gamma_5 = i[\gamma_1, \gamma_2] = 2$. F_V and F_M are the isovector Dirac and Pauli nucleon form factors, taken from Ref.[6]. F_A and F_P are axial and pseudo-scalar form factors, parametrized as

$$F_A(Q^2) = \frac{F_A(0)}{(1 + Q^2/M_A^2)^2}; \quad F_P(Q^2) = \frac{2M F_A(Q^2)}{m^2 + Q^2}; \quad (9)$$

where $F_A(0) = 1.267$, m is pion mass, and $M_A = 1.032 \text{ GeV}$ is axial mass.

The general covariant form of the nuclear tensors is obtained in terms of two four-vectors, namely the four-momenta of target p and q . The electromagnetic and charged-current nuclear tensors can be written as

$$W^{(el)} = W_1^{(el)} g + \frac{W_2^{(el)}}{m_A^2} q q + \frac{W_3^{(el)}}{m_A^2} p p + \frac{W_4^{(el)}}{m_A^2} (p q + q p); \quad (10)$$

$$W^{(cc)} = W_1^{(cc)} g + \frac{W_2^{(cc)}}{m_A^2} q q + \frac{W_3^{(cc)}}{m_A^2} p p + \frac{W_4^{(cc)}}{m_A^2} (p q + q p) + i \frac{W_5}{m_A^2} q p; \quad (11)$$

where W_i are nuclear structure functions which depend on two scalars Q^2 and $p \cdot q$. From Eqs.(10),(11) it follows that in our reference frame $W^{0x}; W^{0y}$, and W^{xz} , vanish together with tensor components obtained from them by exchanging their indices. Therefore, obtained from contraction between lepton Eqs.(3),(4),(5) and nuclear Eqs.(10),(11) tensors, the inclusive cross sections for the QE electron (neutrino)-nucleus scattering are given by

$$\frac{d^{(el)}}{d^3 k_f d} = M (v_L^{(el)} R_L^{(el)} + v_T^{(el)} R_T^{(el)}); \quad (12)$$

$$\frac{d^{(cc)}}{d^3 k_f d} = \frac{G^2 \cos^2 \theta_c}{(2\pi)^2} k_f \mu_f (v_0 R_L^{(cc)} + v_T R_T^{(cc)} + v_{0L} R_{0L}^{(cc)} + v_{LL} R_{LL}^{(cc)} + v_{xy} R_{xy}^{(cc)}); \quad (13)$$

$$M = \frac{2 \cos^2(\theta/2)}{4\pi^2 \sin^4(\theta/2)}; \quad (14)$$

where M is the Mott cross section and θ is the lepton scattering angle. The coefficients $v^{(el)}$ and v are obtained from lepton tensors and can be written as

$$v_L^{(el)} = \frac{Q^4}{4\pi^2}; \quad v_T^{(el)} = \frac{Q^4}{2\pi^2} + \tan^2(\theta/2); \quad (15)$$

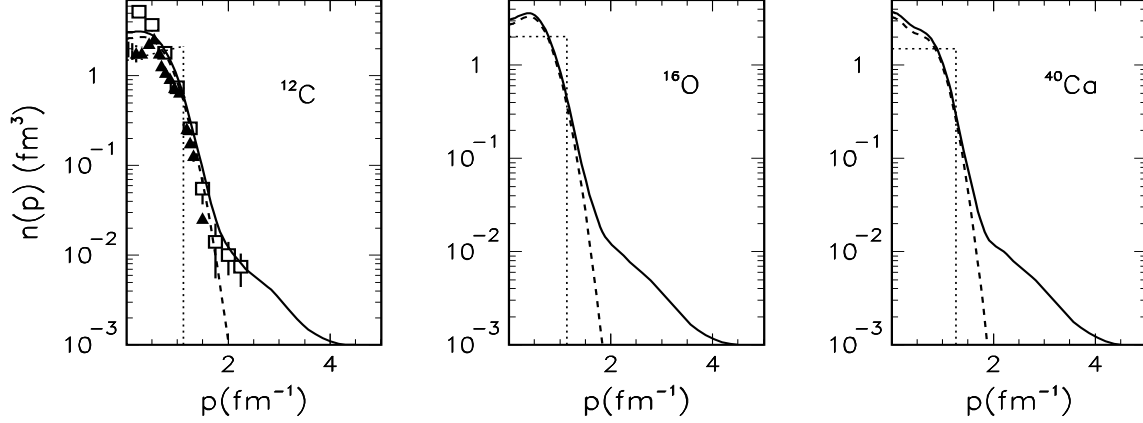


FIG. 1: Nucleon momentum distribution corresponding to Eq.(28) (solid lines) and Eq.(26) (dotted lines). The momentum distribution n_0 is given by short-dashed line. The open squares represent results obtained in Ref.[8]. The full triangles represent the values of $n_0(p)$ obtained in Ref.[9].

$$\begin{aligned}
 v_0 &= 1 + \hat{k} \cos \theta; \\
 v_T &= 1 + \hat{k} \cos \theta + \frac{m_1^2}{2J_f^2} \sin^2 \theta; \\
 v_{0L} &= \frac{1}{2J_f} (1 + \hat{k} \cos \theta) + \frac{m_1^2}{2J_f^2}; \\
 v_{LL} &= 1 + \hat{k} \cos \theta - 2 \frac{m_1^2}{2J_f^2} \sin^2 \theta; \\
 v_{xy} &= \frac{m_1^2}{2J_f} (1 + \hat{k} \cos \theta) - \frac{m_1^2}{2J_f^2}; \quad (16)
 \end{aligned}$$

where $\hat{k} = \mathbf{k}_f / J_f$. The nuclear response functions $R^{(el)}$ and $R^{(cc)}$ are given in terms of components of nuclear tensors as follows [4],[7]

$$\begin{aligned}
 R_L^{(el)} &= W_{00}^{(el)} = \frac{J_f^2}{Q^2} W_1^{(el)} + W_2^{(el)}; \\
 R_T^{(el)} &= W_{xx}^{(el)} + W_{yy}^{(el)} = 2W_1^{(el)} + W_3^{(el)}; \\
 R_L^{(cc)} &= W_{00}^{(cc)} = W_1^{(cc)} + \frac{1}{m_A^2} W_2^{(cc)} + W_3^{(cc)} \\
 &\quad + \frac{2!}{m_A} W_4^{(cc)}; \\
 R_{0L}^{(cc)} &= W_{0z}^{(cc)} + W_{z0}^{(cc)} = \frac{2J_f^2}{m_A^2} (W_2^{(cc)} + m_A W_4^{(cc)}); \\
 R_T^{(cc)} &= W_{xx}^{(cc)} + W_{yy}^{(cc)} = 2W_1^{(cc)}; \\
 R_{LL}^{(cc)} &= W_{zz}^{(cc)} = W_1^{(cc)} + \frac{J_f^2}{m_A^2} W_2^{(cc)}; \\
 R_{xy}^{(cc)} &= \frac{2J_f^2}{m_A} W_5^{(cc)}; \quad (18)
 \end{aligned}$$

In order to evaluate nuclear response functions we consider the RFGM and PWIA approach based on assumption that the virtual photon interacts with o -shell nucleon and neglecting interaction of the knocked out nucleon with the residual nucleus. In the PWIA the four-momenta of the initial nucleus A , the bound o -shell nucleon N , and the final state B are

$$\begin{aligned}
 p_A &= (m_A; 0); \quad p_N = (m_N; (\mathbf{p}^2 + m_N^2)^{1/2}; \mathbf{p}); \\
 p_B &= ((\mathbf{p}^2 + m_B^2)^{1/2}; \mathbf{p});
 \end{aligned}$$

respectively. Here $m_B = m_N + \epsilon$, m_N and ϵ are the mass and intrinsic energy of the final $(A-1)$ -nucleon state, respectively. Within the above assumption the nuclear structure functions can be written as follows

$$\begin{aligned}
 W_i^A^{(el)} &= \int d\mathbf{p} \int dE \sum_{j=1}^Z S^p(\mathbf{p}; E) \sum_{j=1}^{X^2} C_{ij} W_j^{p,off}(Q^2) \\
 &\quad + \text{similar terms for the neutrons}, \quad (19)
 \end{aligned}$$

$$\begin{aligned}
 W_i^A^{(cc)} &= \int d\mathbf{p} \int dE \sum_{j=1}^Z S^n(\mathbf{p}; E) \sum_{j=1}^{X^5} D_{ij} W_j^{n,off}(Q^2); \quad (20)
 \end{aligned}$$

Here, Z is the number of protons, $W_j^{N,off}$ ($N = p, n$) are the o -shell nucleon structure functions that are given in the terms of nucleon form-factors. $S^N(\mathbf{p}; E)$ is the nucleon spectral function and kinematic factors C_{ij}, D_{ij}

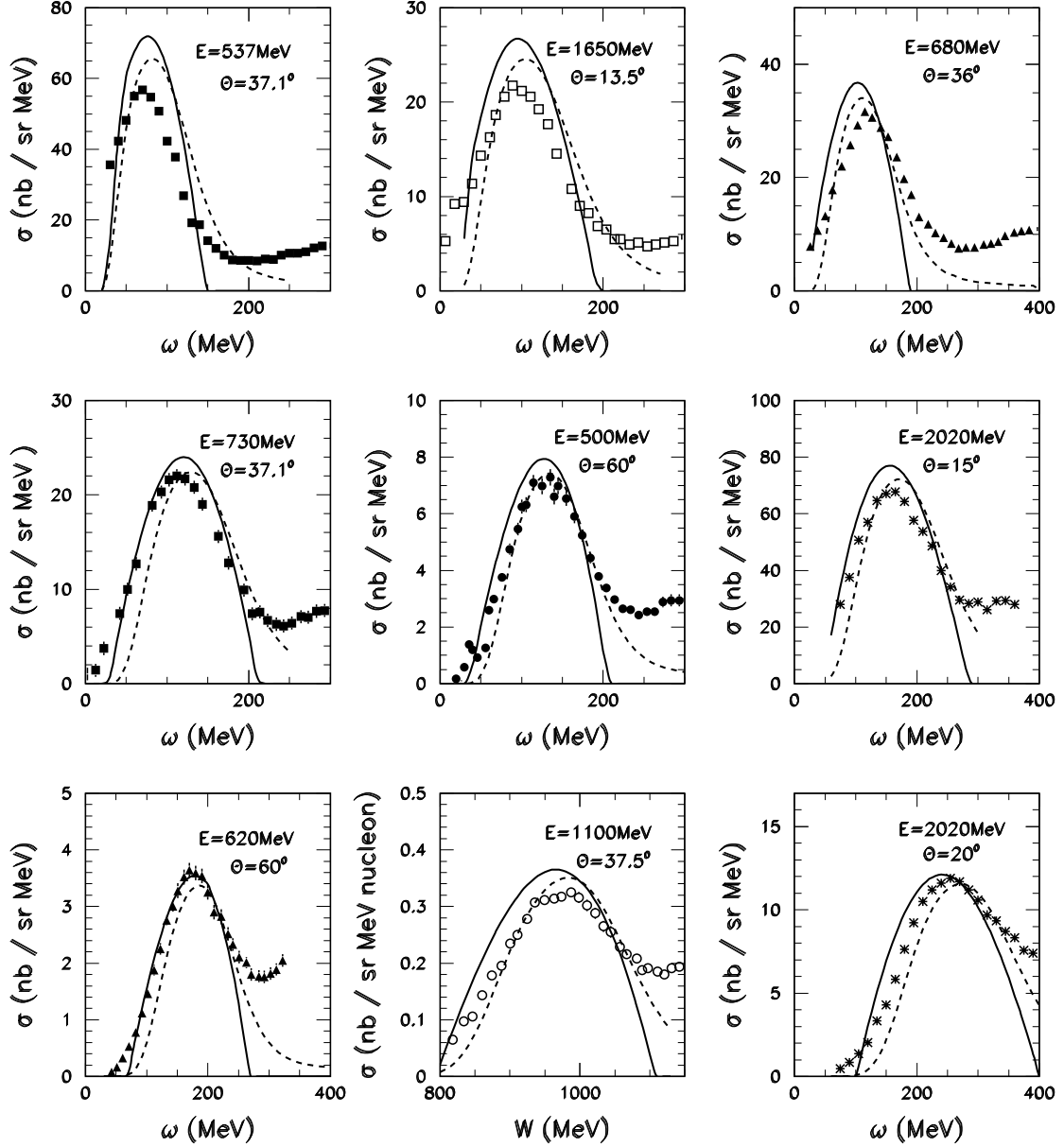


FIG. 2: Comparison of theoretical and experimental cross sections for ^{12}C . The data are taken from Refs.[10] (filled circles), [11] (filled squares), [12] (filled triangles), [13] (open circles), [14] (open squares), and [15] (stars).

have from

$$C_{11} = 1; \quad C_{12} = \frac{1}{2M^2} \left(\frac{pq}{\hbar^2} + \frac{1}{2M^2} \right); \quad C_{21} = 0;$$

and

$$D_{11} = 1; \quad D_{13} = \frac{pq}{2M^2} (1 - \cos^2 \theta);$$

$$D_{12} = D_{14} = D_{15} = 0;$$

$$C_{22} = \frac{1}{M^2} \left(p_0^2 + 2p_0 \frac{pq}{\hbar^2} + \frac{1}{2M^2} \frac{pq}{\hbar^2} \right) + \frac{Q^2}{\hbar^2} C_{12};$$

(21)

$$D_{22} = \frac{m_A^2}{M^2}; \quad D_{23} = \frac{pq m_A^2 (3 \cos^2 \theta - 1)}{2M^2 \hbar^2};$$

$$D_{24} = 2 \frac{m_A}{M} \frac{pq}{\hbar^2} \cos \theta; \quad D_{21} = D_{25} = 0;$$

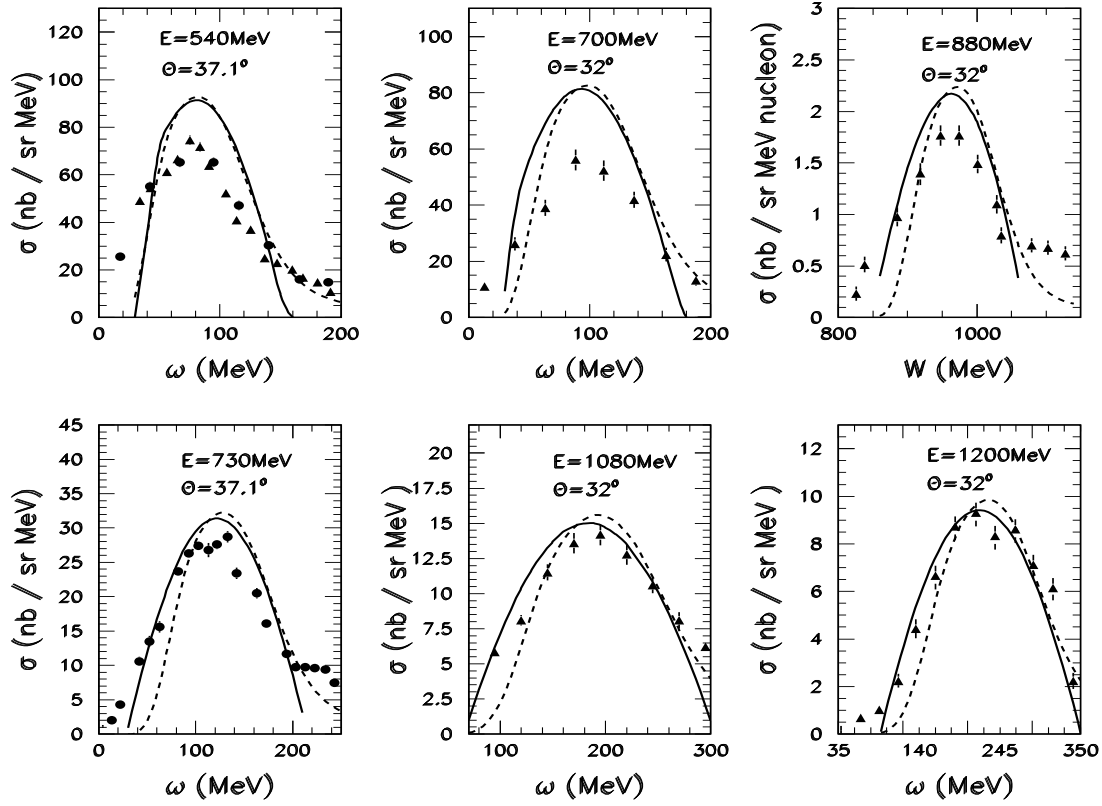


FIG . 3: Comparison of theoretical and experimental cross sections for ^{16}O . The data are taken from Refs.[11] (filled circles), and [16] (filled triangles).

$$D_{33} = \frac{\mathbf{p} \cdot \mathbf{j}}{2M^2} \left(1 - \frac{|\mathbf{j}|^2}{\mathbf{j} \cdot \mathbf{j}} \right) (1 - \cos^2 \theta) + \frac{\mathbf{p} \cdot \mathbf{j} |\mathbf{j}|^2 \cos^2 \theta}{M^2 \mathbf{j} \cdot \mathbf{j}} + \frac{2p_0 |\mathbf{j}| \cdot \mathbf{p} \cdot \mathbf{j} \cos \theta}{M^2 \mathbf{j} \cdot \mathbf{j}} + \frac{p_0^2}{M^2};$$

$$D_{31} = D_{32} = D_{34} = D_{35} = 0;$$

$$D_{43} = \frac{m_A}{M^2} \frac{p_0 \mathbf{p} \cdot \mathbf{j} \cos \theta}{\mathbf{j} \cdot \mathbf{j}} - \frac{|\mathbf{p} \cdot \mathbf{j}|^2}{2\mathbf{j} \cdot \mathbf{j}} (3\cos^2 \theta - 1);$$

$$D_{44} = \frac{m_A}{M^2} p_0 + \frac{|\mathbf{p} \cdot \mathbf{j}| \cos \theta}{\mathbf{j} \cdot \mathbf{j}}; \quad D_{41} = D_{42} = D_{45} = 0;$$

$$D_{51} = D_{52} = D_{53} = D_{54} = 0;$$

$$D_{55} = \frac{m_A}{M^2} p_0 + \frac{|\mathbf{p} \cdot \mathbf{j}| \cos \theta}{\mathbf{j} \cdot \mathbf{j}}; \quad (22)$$

as follows

$$W_1^{N(e1)} = \frac{Q^2}{4p_0 p_0^0} [F_V(Q^2) + F_M(Q^2)]^2 (p_0 + |\mathbf{p}| p_0^0); \quad (23)$$

$$W_2^{N(e1)} = \frac{M^2}{p_0 p_0^0} [F_V^2(Q^2) + \frac{Q^2}{4M^2} F_M^2(Q^2)] (p_0 + |\mathbf{p}| p_0^0); \quad (24)$$

and

$$W_j^{n(cc)} = \frac{1}{2p_0 p_0^0} \bar{W}_j (p_0 + |\mathbf{p}| p_0^0); \quad (25)$$

with

$$\bar{W}_1 = \frac{Q^2}{2} (F_V + F_M)^2 + F_A^2 \left(1 + \frac{4M^2}{Q^2} \right);$$

$$\bar{W}_3 = 2M^2 F_V^2 + \frac{Q^2}{4M^2} F_M^2 + F_A^2;$$

$$\bar{W}_2 = \frac{1}{4} \bar{W}_3 \left[\frac{M^2}{Q^2} \bar{W}_1 + \frac{2}{Q^2} F_A + \frac{Q^2}{2M^2} F_P^2 \right];$$

$$\bar{W}_4 = \frac{1}{2} \bar{W}_3; \quad \bar{W}_5 = 2M^2 F_A (F_V + F_M); \quad (26)$$

where $\cos \theta = \mathbf{p} \cdot \mathbf{q} / |\mathbf{p}| |\mathbf{q}|$. In this paper we assume that $W_j^{N,off}$ are identical to free nucleon structure function W_j^N . The parametrization of W_j^N is taken from Refs.[2,3]

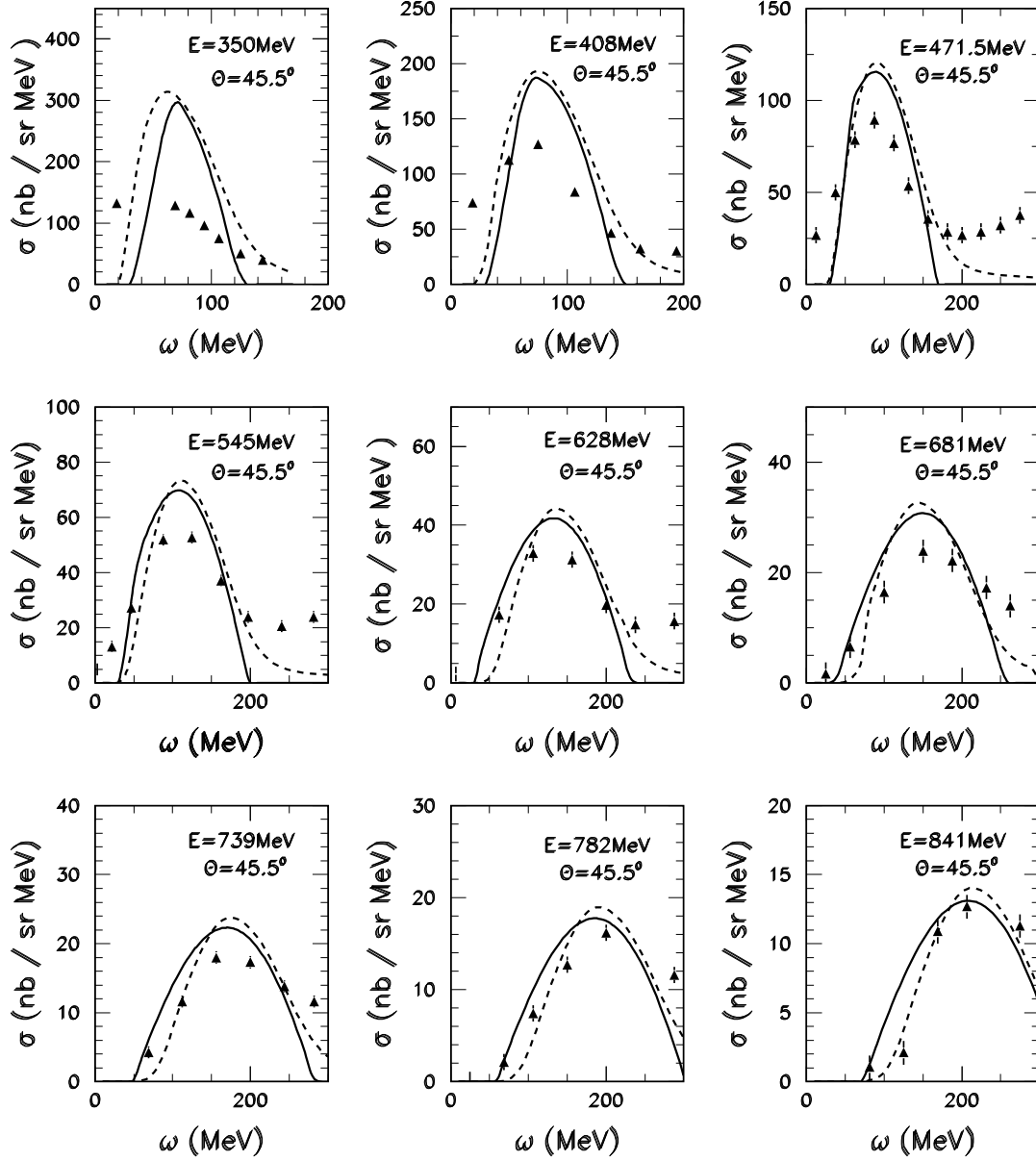


FIG. 4: Comparison of theoretical and experimental cross sections for ^{40}Ca . The data are taken from Ref.[18].

where $p_0^0 = [(\mathbf{p} + \mathbf{q})^2 + M^2]^{1/2}$ is energy of the knocked-out nucleon.

The nucleon spectral function $S^N(\mathbf{p}; E)$ in the PW IA represents probability to find the nucleon with the momentum \mathbf{p} and the removal energy E in the ground state of the nucleus. In the commonly used Fermi gas model, that was described by Smith and Moniz [2], nucleons in nuclei are assumed to occupy plane wave states in uniform potential while the knocked-out nucleon is outside of the Fermi sea. The Fermi gas model provides the sim-

plest form of the spectral function which is given by

$$S_{FG}(E; \mathbf{p}) = \frac{3}{4 p_F^3} (\mathbf{p}_F - \mathbf{p}) \cdot (\mathbf{p} + \mathbf{q} - \mathbf{p}_F) \cdot [(\mathbf{p}^2 + M^2)^{1/2} - \epsilon_b - E]; \quad (27)$$

where p_F denotes the Fermi momentum and a parameter ϵ_b is effective binding energy, introduced to account of nuclear binding. The QE lepton-nucleus reactions are complicated processes, involving nuclear many body effects. The calculation of the nuclear spectral function for complex nuclei requires to solve many body problem. In

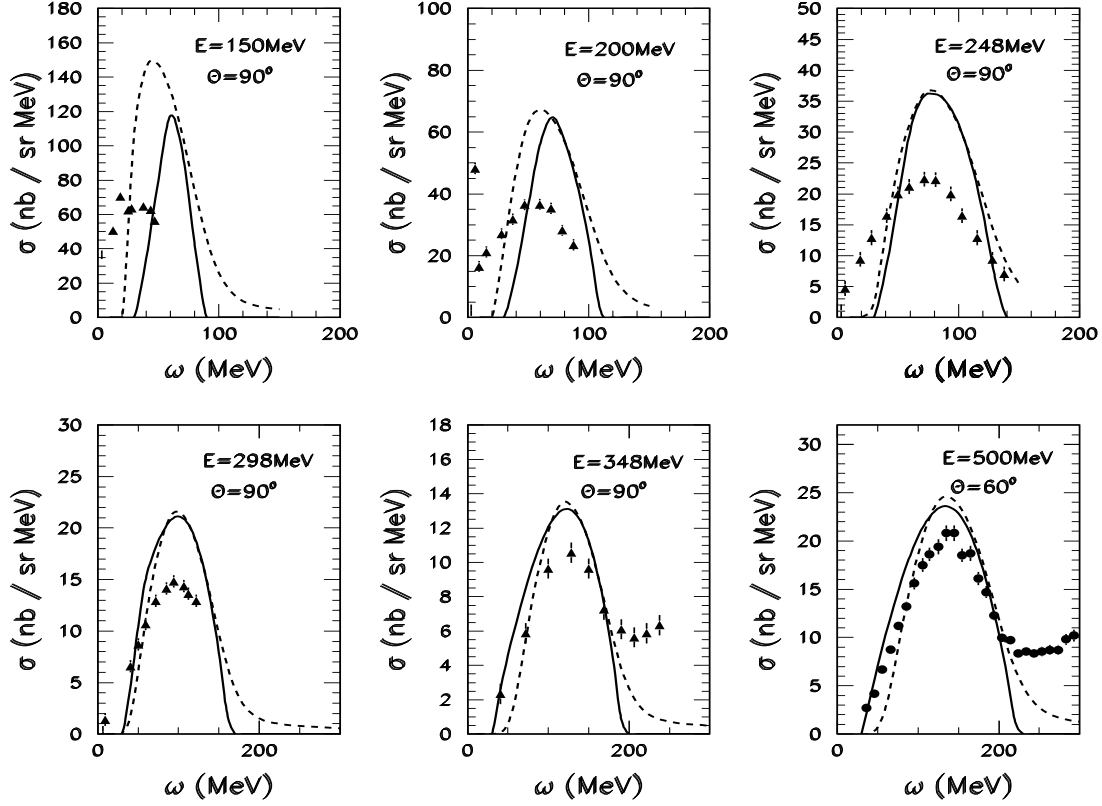


FIG. 5: Comparison of theoretical and experimental cross sections for ^{40}Ca . The data are taken from Refs. [10] (filled circles), and [18] (filled triangles).

In this paper we consider also a phenomenological model using PWIA approach with the spectral function which incorporates both the single particle nature of the nucleon spectrum at low energy and high-energy and high momentum components due to NN-correlations in ground state. Following [4,5] we separate the full spectral function into two parts

$$S(E; p) = S_0(E; p) + S_1(E; p); \quad (28)$$

The integration of Eq.(27) over energy gives nucleon momentum distribution,

$$n(p) = \int \frac{dE}{2} S(E; p) = n_0(p) + n_1(p); \quad (29)$$

The spectral function is normalized according to

$$\int \frac{dE dp}{2} S(E; p) = 1; \quad (30)$$

The low-energy part (S_0) can be approximated by the following expression

$$S_0(E; p) = 2 n_0(p) (E - \epsilon^{(1)}) p^2 = 2M_A \epsilon^{(1)}; \quad (31)$$

with $\epsilon^{(1)}$ the nucleon separation energy averaged over residual configurations of $A-1$ nucleons with low excitation energies and recoil energy $p^2 = 2M_A \epsilon^{(1)}$, $n_0(p)$ is the corresponding part of nucleon momentum distribution.

The high-excitation part (S_1) of the spectral function is determined by excited states with one or more nucleons in continuum. The detailed description of this model is given in Refs.[4,5] as well as parametrization of $n_0(p)$ and $n_1(p)$, which is the result of many-body calculations of nucleon momentum distribution. As follows from these calculations the low momentum part incorporates about 80% of the total normalization of spectral function, while the other 20% are taken by the high momentum part. The nucleon momentum distributions $n(p)$ and $n_{FG}(p)$ are shown in Fig.1. The normalization of $n(p)$ and $n_{FG}(p)$ is $\int dp p^2 n(p) = 1$, where $p = |p|$. The distributions n_{FG} for various nucleus ^{12}C , ^{16}O and ^{40}Ca were calculated using the value of parameters $p_F = 221 \text{ MeV}$, $b = 25 \text{ MeV}$ (^{12}C); $p_F = 225 \text{ MeV}$, $b = 27 \text{ MeV}$ (^{16}O); and $p_F = 249 \text{ MeV}$, $b = 33 \text{ MeV}$ (^{40}Ca) [10].

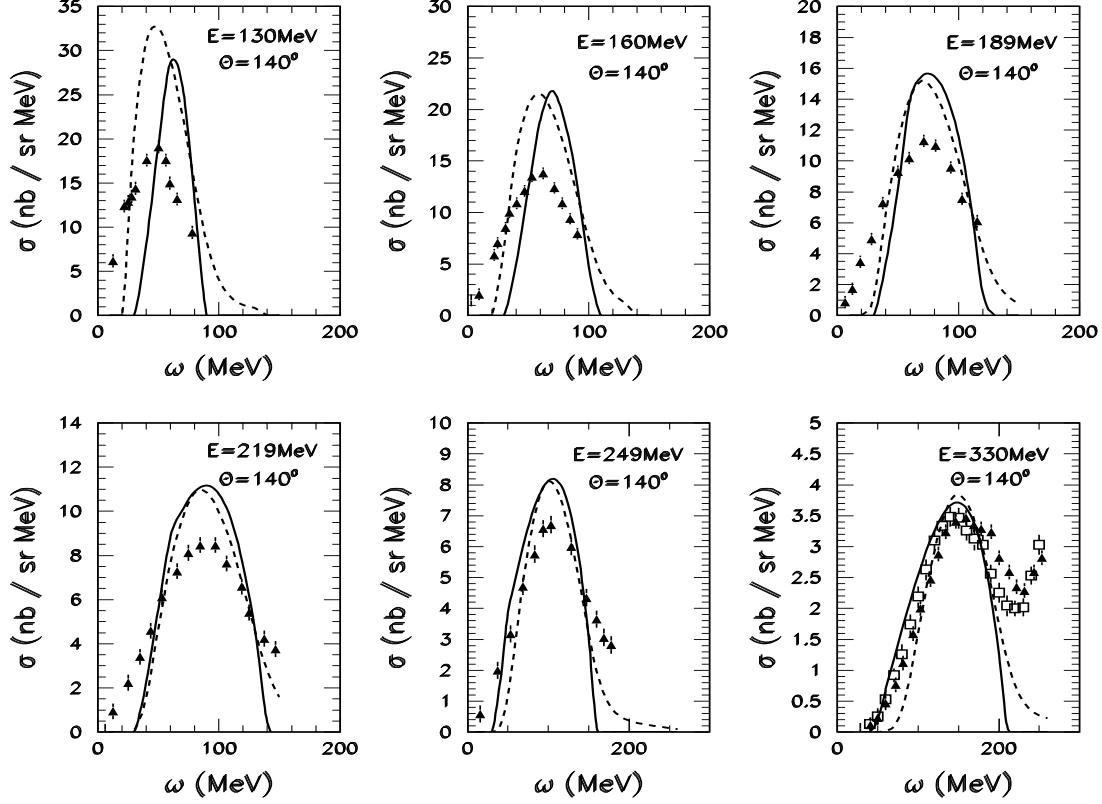


FIG. 6: Comparison of theoretical and experimental cross sections for ^{40}Ca . The data are taken from Refs. [17] (open squares), and [18] (filled triangles).

III. RESULTS

There is vast high-precision data for electron scattering on nucleus ^{12}C , ^{16}O , and ^{40}Ca . Hence these nuclei are taken at the focus of the present work. Data on inclusive cross sections for a number of nuclei (A between 6 and 208) but only one set of kinematics were obtained early in Ref. [10]. Carbon data are available from experiments [11]–[15]. For oxygen target the experiments were performed by SLAC [11] and Frascati [16] groups. For calcium target the inclusive cross section have been measured in experiments [10], [17]–[19]. All these data were used in our analysis.

Using both the relativistic Fermi gas model and the PWIA approach described above, we calculated the inclusive cross sections for given kinematics (energies and angles) and compared them with data. The results are presented in Figs. 2–6 for ^{12}C , ^{16}O , and ^{40}Ca respectively. The solid lines are the results in the Fermi gas model, while short-dashed lines are results in the PWIA. The differences can be seen from these figures in which the cross sections as functions of Q^2 or invariant mass produced on a free nucleon W are plotted. At the maximum of

the cross sections both models overestimate the measured values. We evaluated the differences between predicted (σ_{calc}) and measured (σ_{data}) quantities $\sigma_{\text{calc}} - \sigma_{\text{data}}$ as a function of three-momentum transfer q is shown in Fig. 7, from which it is clear that the (q) decreases with q from 30–50% at $q \approx 200$ MeV to 10–15% at $q \approx 500$ MeV.

In Refs. [17], [18] transverse $R_T^{(\text{el})}$ and longitudinal $R_L^{(\text{el})}$ response functions have been extracted for 200 MeV q 500 MeV. It has been shown that the RFGM overestimates the observed longitudinal response for about 40% [17] (20% [18]). At low q this model also overestimates the magnitude of the transverse response function. At higher values of q it does better at reproducing the value of the $R_T^{(\text{el})}$.

The predictions of both models are compared with the experimental result of the LSND collaboration at Los Alamos for $^{12}\text{C}(\nu; \mu)$ reaction [20]. The calculations are flux-averaged over the Los Alamos neutrino flux. The mean energy of neutrino flux above threshold is 156 MeV. The comparison is shown in Fig. 8 where the calculated muon energy distributions are normalized to the experimental total number events. We note that

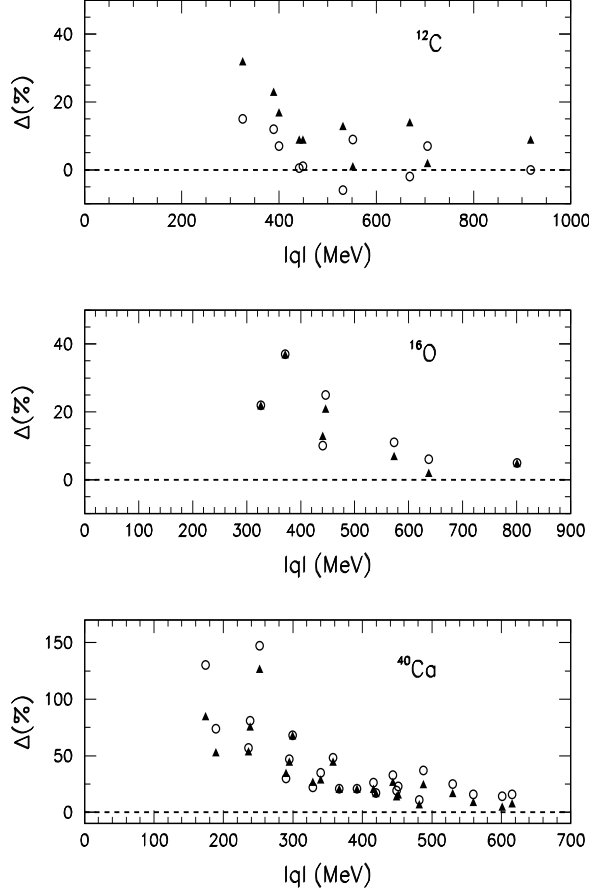


FIG. 7: Differences between calculated and measured values of cross sections at maximum for ^{12}C , ^{16}O , and ^{40}Ca as functions of three-momentum transfer $|\mathbf{q}|$. The filled triangles correspond to the Fermi gas model results and open circles correspond to the PWIA approach.

both models do not give an accurate descriptions of the shape of the muon spectrum. The flux-averaged cross section integrated over the muon energy is $17.8 \cdot 10^{40} \text{ cm}^2$ in the case of the RFGM and $26.8 \cdot 10^{40} \text{ cm}^2$ in the PWIA. The experimental value is $(10.6 \pm 0.3 \pm 1.8) \cdot 10^{40} \text{ cm}^2$. The result obtained by other calculation in the framework of the Fermi gas model with local density approximation [21] gives also larger value $= (16.7 \pm 1.37) \cdot 10^{40} \text{ cm}^2$.

IV. CONCLUSIONS

In this work we have tested the widely used relativistic Fermi gas model and plane-wave in pulse approximation approach against electron-nucleus scattering data. We calculated the inclusive QE cross sections and com-

pared them with high-precision data for ^{12}C , ^{16}O , and

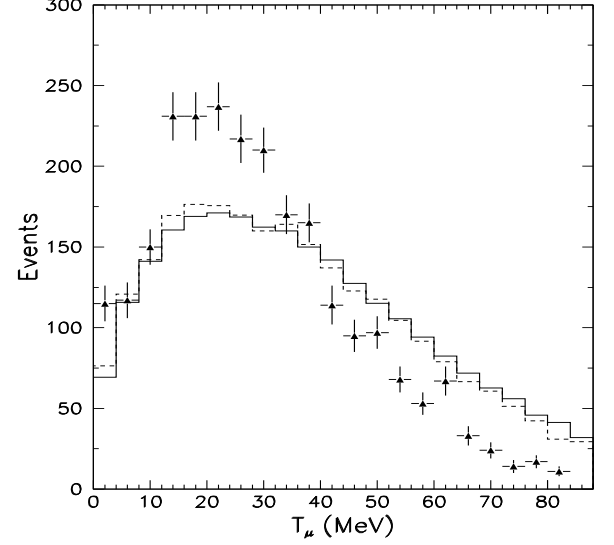


FIG. 8: The distribution of muon kinetic energy for inclusive $^{12}\text{C} (;)$ reaction. Experimental data from Ref.[20]. The results of the RFGM (solid line histogram) and the PWIA approach (short-dashed line histogram) are normalized to the data.

^{40}Ca in a wide region of incident energy and momentum. We evaluated the differences between predicted and measured QE cross section at the maximum and found that both models overestimate the measured values. The function $(\mathbf{q}|\mathbf{q})$ decreases with three-momentum transfer from 30-50% at $|\mathbf{q}| = 200 \text{ MeV}$ to 10-15% at $|\mathbf{q}| = 500 \text{ MeV}$. Therefore these models overestimate also the cross sections at low $Q^2 = |\mathbf{q}|^2 - \mu^2$.

We applied the RFGM and PWIA approach to $^{12}\text{C} (;)$ reaction. The flux-averaged total cross sections and muon energy distributions were calculated and compared with experimental results of the LSND collaboration. The calculated cross sections are significantly larger than the experimental ones and both models do not give an accurate description of the shape of muon spectrum.

In conclusion we note that the inclusion of final state interaction effects along with realistic spectral function may significantly correct the description of the data at low momentum transfer, as was pointed in Ref.[16].

Acknowledgments

This work was supported by the Russian Foundation for Basic Research project No 02-02-17036. We would like to thank S. Kulagin for fruitful discussions.

-
- [1] G.P. Zeller, arXiv:hep-ex/0312061.
- [2] R.A. Smith, and E.J. Moniz, Nucl. Phys. B 101, 547, 1975.
- [3] J.J. Kelly, Adv. Nucl. Phys. 23, 75, 1996.
- [4] C. Cio degli Atti, and S. Simula, Phys. Rev. C 53, 1689, 1996.
- [5] S.A. Kulagin, and R. Petti, arXiv:hep-ph/0412425.
- [6] M.J. Musolf, and T.W. Donnelly, Nucl. Phys. A 546, 509, 1992.
- [7] A. Mucci, C. Giusti, and D. Pacati, Nucl. Phys. A 739, 277, 2004.
- [8] C. Cio degli Atti, E. Pace, and G. Salme, Phys. Rev. C 43, 1153, 1991.
- [9] S. Frullani, and J. Mougey, Adv. Nucl. Phys. 14, 1, 1981.
- [10] R. Whitney et al., Phys. Rev. C 9, 2230, 1974.
- [11] J.S. O'Connell et al., Phys. Rev. C 35, 1063, 1987.
- [12] P. Barreau et al., Nucl. Phys. A 402, 515, 1983.
- [13] R.M. Sealock et al., Phys. Rev. Lett. 62, 1350, 1989.
- [14] D. Baran et al., Phys. Rev. Lett. 61, 400, 1988.
- [15] D. Day et al., Phys. Rev. C 48, 1819, 1993.
- [16] M. Anghinol et al., Nucl. Phys. A 602, 402, 1996.
- [17] M. Dedy et al., Phys. Rev. C 33, 1987, 1986.
- [18] C. Williamson et al., Phys. Rev. C 56, 3152, 1997.
- [19] Z. Meziani et al., Phys. Rev. Lett. 54, 1233, 1985.
- [20] L.B. Auerbach et al., Phys. Rev. C 66, 015501, 2002.
- [21] S.K. Singh, N.C. Mukhopadhyay, and E. Oset, Phys. Rev. C 57 2687, 1998.